

Research Article

Performance of Partial and Cavity Type Squealer Tip of a HP Turbine Blade in a Linear Cascade

Levent Kavurmacioglu¹, Hidir Maral,¹ Cem Berk Senel¹, and Cengiz Camci^{1,2}

¹Department of Mechanical Engineering, Istanbul Technical University, Istanbul, Turkey

²Department of Aerospace Engineering, Turbomachinery Aero-Heat Transfer Laboratory, The Pennsylvania State University, University Park, PA, USA

Correspondence should be addressed to Cengiz Camci; cxc11@psu.edu

Received 7 September 2017; Accepted 17 December 2017; Published 2 May 2018

Academic Editor: Xuefeng Zhang

Copyright © 2018 Levent Kavurmacioglu et al. This is an open access article distributed under the Creative Commons Attribution License, which permits unrestricted use, distribution, and reproduction in any medium, provided the original work is properly cited.

Three-dimensional highly complex flow structure in tip gap between blade tip and casing leads to inefficient turbine performance due to aerothermal loss. Interaction between leakage vortex and secondary flow structures is the substantial source of that loss. Different types of squealer tip geometries were tried in the past, in order to improve turbine efficiency. The current research deals with comparison of partial and cavity type squealer tip concepts for higher aerothermal performance. Effects of squealer tip have been examined comprehensively for an unshrouded HP turbine blade tip geometry in a linear cascade. In the present paper, flow structure through the tip gap was comprehensively investigated by computational fluid dynamic (CFD) methods. Numerical calculations were obtained by solving three-dimensional, incompressible, steady, and turbulent form of the Reynolds-averaged Navier-Stokes (RANS) equations using a general purpose and three-dimensional viscous flow solver. The two-equation turbulence model, shear stress transport (SST), has been used. The tip profile belonging to the Pennsylvania State University Axial Flow Turbine Research Facility (AFTRF) was used to create an extruded solid model of the axial turbine blade. For identifying optimal dimensions of squealer rim in terms of squealer height and squealer width, our previous studies about aerothermal investigation of cavity type squealer tip were utilized. In order to obtain the mesh, an effective parametric generation has been utilized using a multizone structured mesh. Numerical calculations indicate that partial and cavity squealer designs can be effective to reduce the aerodynamic loss and heat transfer to the blade tip. Future efforts will include novel squealer shapes for higher aerothermal performance.

1. Introduction

In order to allow the relative motion of blades and to prevent the blade tip surface from rubbing, clearance gap between blades and casing is required in turbomachinery. The overall performance of turbomachines is strongly related to the flow within tip gap. The flow in this gap is 3D and highly recirculatory. The pressure difference across the pressure and suction side of blades forms a leakage flow passed over the blade tip surface. This pressure-driven leakage flow throughout the gap results in approximately one-third of the aerodynamic losses in the rotor of an axial flow gas turbine [1]. The flow structure in the tip gap is a significant source of inefficiency in terms of aerodynamic loss and heat transfer to the blade tip and casing. The leakage flow passes over the blade

tip without being turned and expanded as the passage flow; thus, a reduction in useful work extracted from the turbine is observed [1, 2]. The leakage flow is also a significant source of higher local thermal loads on the blade tip platform which is exposed to the hot gas stream [3]. There are many studies in order to clarify the structure of the tip leakage flow and to reduce its adverse effects. In an early investigation, Moore and Tilton [4] investigated the leakage flow both analytically and experimentally considering the flow through the tip gap as a flow through an orifice. Bindon [5] revealed the effects of tip geometries and radius at the pressure side corner on aerodynamic loss. Yaras and Sjolander [6] investigated the effect of relative motion between blades and casing and experiments revealed that the leakage flow rate was decreased by the effect of rotation.

Passive control methods such as squealer, partial squealer, and winglet blade tip designs are widely used in order to reduce the effects of leakage flow. Heyes et al. [2] figured out that the implementation of squealer tip geometries could be effective in reducing the leakage flow since a separation bubble in the cavity partially blocks the flow. Ameri et al. [7] numerically investigated the effect of a squealer geometry on heat transfer and efficiency and obtained that the leakage flow rate was reduced, whereas the heat transfer to the blade tip was increased. Numerical results showed that a cavity squealer reduced aerodynamic loss and heat transfer to the blade tip. In this study, it was stated that the width of the squealer could be effective in determining the performance of the squealer. Newton et al. [8] performed an experimental investigation for flat tip, suction side squealer, and cavity squealer in a linear cascade. Their results revealed that a reduction in heat transfer to the blade tip was obtained. Camci et al. [9] experimentally studied the aerodynamic characteristics of partial squealer rims in the single-stage, low-speed, rotating Axial Flow Turbine Research Facility (AFTRF) of the Pennsylvania State University and found that the suction side squealer had a better aerodynamic performance with respect to cavity squealer. Krishnababu et al. [10] performed a numerical investigation on the effects of blade tip geometry and found that cavity tip improved the aerodynamic performance and decreased the heat transfer rates to the blade tip. Kavurmacioglu et al. [11] and Kavurmacioglu et al. [12] carried out a numerical study in a rotational test rig (AFTRF) for aerodynamic performance of full- and partial-length squealer rims. Li et al. [13] simulated the aerodynamic performance of five passive control methods: pressure side winglet, suction side winglet, cavity squealer, inclined pressure side squealer, and partial suction side squealer tip. They revealed that inclined pressure side squealer had the best turbine efficiency. Lee and Kim [14] investigated the flow structure over a cavity squealer tip experimentally for a linear turbine cascade. Zhou and Hodson [15] studied on the aero-thermal performance of a cavity squealer rim with two different widths and heights in a subsonic linear cascade both experimentally and numerically. Liu et al. [16] performed a numerical investigation on the flow and heat transfer for various blade tip designs comprising pressure side, suction side, and cavity squealer tips and obtained that cavity squealer had minimum aerodynamic loss while pressure side squealer provided minimum heat transfer to the blade tip. Schabowski and Hodson [17] found lower aerodynamic loss in the case of cavity squealer compared to the suction side squealer by their numerical and experimental studies. Ma and Wang [18] studied the aerodynamic effects of various tip designs including pressure side, suction side, and cavity squealer tip geometries in a low-speed turbine cascade. Their results showed that cavity squealer tip provided lower aerodynamic loss. Recently, Maral et al. [19] performed a numerical study on aero-thermal characteristics of flat, cavity, and suction side partial squealer blade tips. They found that the cavity squealer provides the lowest aerodynamic loss while the suction side partial squealer provides the lowest heat transfer to the blade tip.

In this paper, effects of the squealer tip section have been examined comprehensively for an unshrouded HP turbine blade in a linear cascade. A special emphasis is placed in obtaining three-dimensional and complex mesh systems in a parametric effort. The parametric approach in tip leakage mitigation studies provides significant time savings for the construction of the solid model and its associated mesh. Conceptual view of flat, partial squealer and cavity squealer tip designs is shown in Figure 1.

2. Numerical Method

A numerical study has been conducted in the present paper using computational fluid dynamics (CFD) that is an important tool to make a better understanding flow in turbomachines, especially where experimental measurements may become difficult, expensive, and time-consuming.

Three different tip designs are investigated: flat tip (FLAT), cavity squealer (SQ), and suction side partial squealer (PSQ). The HP turbine blade profile used in this numerical study belongs to the Axial Flow Turbine Research Facility (AFTRF) of Camci [20] at the Pennsylvania State University. The original tip profile of the AFTRF rotor airfoil is used to form an extruded solid model of the blade tip for the current computations. Some of the design features of turbine blade is given in Table 1. A sketch depicting the geometrical parameters of the linear cascade arrangement is shown in Figure 2 and the manufacturing coordinates of the tip airfoil section are given in Table 2. In this study, the squealer height is 0.615 mm while the tip gap height is 0.615 mm which corresponds to a tight tip clearance ($t/h = 0.5\%$). The width of the squealer has been defined as 0.4 mm. Computational domain is obtained in ANSYS SpaceClaim as a linear cascade arrangement. Computational domain for the squealer tip is given in Figure 3. There are three basic domains: inlet, blade, and outlet. Inlet length is defined as one axial chord while outlet length is equal to two axial chords. Length of the inlet and outlet domains is defined as $1C_a$ and $2C_a$, respectively.

Blade domain is divided into 9 blocks to generate a fully hexagonal mesh in a simple way. As shown in Figure 4(a), fully hexagonal elements are used in the calculations to reduce solution time and obtain more accurate results. Creating multiblocked flow domain enables to use multizone method in ANSYS meshing module. Multizone method can be defined as a type of blocking approach similar to ICEM-CFD. Automated topology decomposition is used so as to generate structured hexagonal mesh where blocking topology is available [21]. The present study introduces a parametric grid generation approach that is introduced using both the squealer height and the squealer thickness as parameters. The grids for the three different blade tips are obtained using this parametric approach. This is the first paper in a series of publications for the current tip leakage mitigation research effort. Figure 4(b) shows the fully hexagonal surface grid structure of the whole turbine blade. This grid automation effort saves a significant amount of time in all phases of this program. Also, a boundary layer mesh using an O-grid topology is utilized to keep y^+ at a desired level of approximately 1 in the present effort. The tip gap region is divided into two

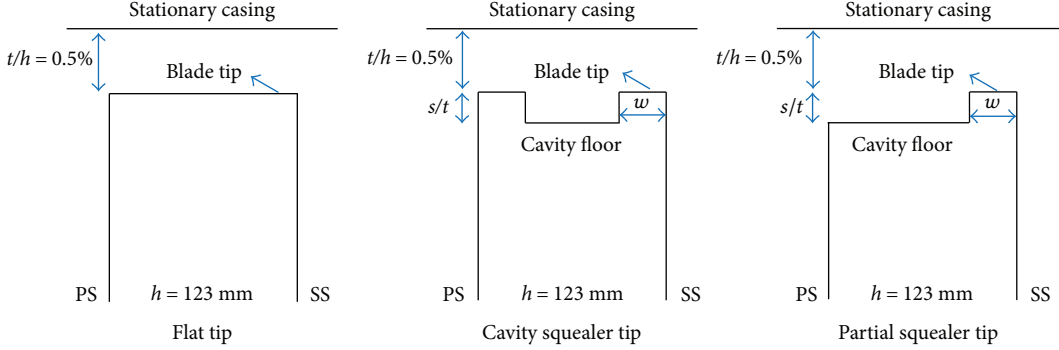


FIGURE 1: Conceptual view of blade tip designs.

TABLE 1: AFTRF rotor blade specifications.

Blade height (mm)	123.615
Tip gap height (mm)	0.615
Chord (mm)	121.5
Axial chord (mm)	85.04
Inlet flow angle, α ($^{\circ}$)	71.3
Pitch, p (mm)	99.274
Stagger angle, ζ ($^{\circ}$)	46.2

subdomains named squealer and tip gap. These two subdomains are also separated into multiblocks. The number of divisions in tip gap is selected to be 36 by employing equal divisions. The CFD analysis is conducted using the general purpose flow solver ANSYS CFX 16.0. As soon as the mesh is generated, the mesh file is transferred to CFX-Pre for the modeling and CFX-Solver for the simulation.

The dependency of the current results on grid size was studied for the flat tip section. Three different mesh sizes were investigated by gradual refinements, from a coarse to medium to fine grid structure, as shown in Figure 4(c). Number of divisions in the tip clearance gap for coarse, medium, and fine cases were 30, 35, and 40, respectively. The sensitivity to grid size on the pressure side was minimal. The three grid systems used also showed almost no sensitivity in the first 70% axial chord of the suction side. However, there is an “almost negligible” amount of grid dependency in the last 30% axial chord of the suction side. This specific area corresponds to the slight diffusion zone existing on the suction side.

The mesh dependency of “total pressure” that is a great measure of aerodynamic losses was also examined. The mass-averaged total pressure of the exit plane ($x = 56$ mm downstream of the blade trailing edge) was obtained for coarse, medium, and fine mesh cases. The number of divisions in the tip clearance gap for coarse, medium, and fine grid cases were also 30, 35, and 40. When the computation was carried out using the coarse mesh, the mass-averaged total pressure in exit plane was found to be 99,749 Pa. In the second attempt, the medium mesh resulted in 99,747 Pa. For the highest resolution fine mesh, the exit plane

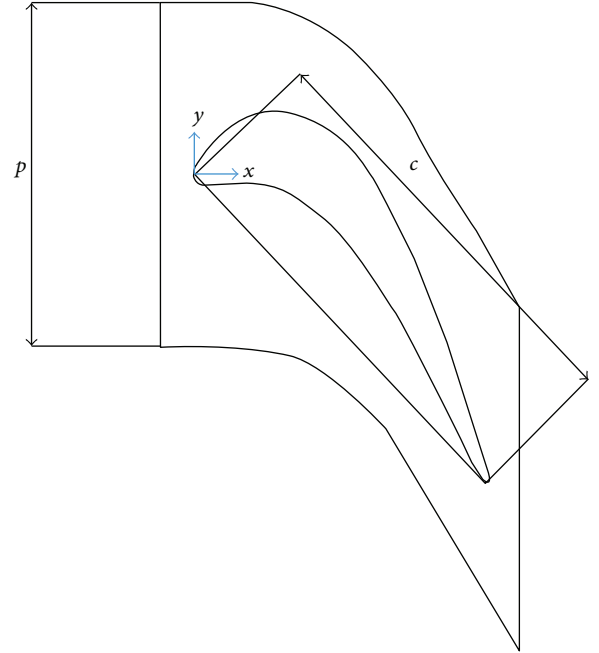


FIGURE 2: Linear cascade arrangement for the AFTRF rotor.

total pressure was obtained as 99,738 Pa. All three computations resulted in very similar exit total pressure values. The worst case deviation from the fine mesh value was 11 Pa. A typical “total pressure” measurement uncertainty for a differential transducer/probe system is about 0.5% ($+/-35$ Pa) in modern aerodynamic laboratories. The worst case computational deviation of 11 Pa from the fine grid was considered to be easily acceptable for the current computations. Although all three mesh sizes used in this study exhibited minimal mesh dependency, the FINE mesh was used for all numerical calculations.

Due to being highly turbulent flow, a two-equation model is used in the calculations. Shear stress transport (SST) turbulence model is performed. SST turbulence model is a combination standard ($k-\epsilon$) and ($k-\omega$) to overcome the shortcomings of each model by a blending function depending on the distance away from the wall [22]. SST turbulence model requires a condition, $y^+ < 2$, that must be satisfied for

TABLE 2: Profile coordinates of turbine rotor tip section.

x (mm)	y (mm)						
-39.921	16.351	42.085	-71.364	-4.310	-4.462	30.965	-28.265
-39.355	18.171	42.452	-72.129	-1.512	1.906	29.330	-23.823
-39.982	15.701	42.808	-72.725	1.224	-0.900	27.590	-19.246
-39.721	17.175	43.160	-73.102	3.813	-3.844	25.791	-14.692
-39.953	15.212	43.503	-73.251	6.276	-6.894	23.922	-10.166
-39.869	14.813	43.827	-73.292	8.623	-10.034	21.923	-5.674
-39.752	14.508	44.086	-73.258	10.878	-13.241	19.925	-1.226
-39.637	14.292	44.274	-73.203	13.038	-16.508	17.772	3.172
-39.526	14.130	44.492	-73.091	15.139	-19.889	15.479	7.499
-39.358	13.930	44.739	-72.878	17.176	-23.170	13.025	11.736
-39.115	13.711	44.966	-72.539	19.159	-26.552	10.379	15.856
-38.792	13.489	45.062	-72.063	21.092	-29.692	7.508	19.823
-38.322	13.261	44.968	-71.420	22.986	-33.394	4.341	23.558
-37.673	13.059	44.744	-70.605	24.845	-36.845	0.816	26.956
-38.838	12.905	44.430	-69.587	26.616	-40.196	-2.982	29.782
-35.808	12.826	44.053	-68.353	28.301	-43.443	-7.031	31.901
-34.580	12.833	43.610	-66.885	29.908	-46.584	-11.229	33.241
-33.145	12.919	43.089	-65.167	31.440	-49.616	-15.434	33.811
-31.452	13.056	42.470	-63.137	32.901	-52.538	-19.512	33.645
-29.497	13.188	41.752	-60.797	34.294	-55.348	-23.339	32.808
-27.277	13.263	40.931	-58.146	35.617	-58.044	-26.810	31.380
-24.794	13.232	40.005	-55.187	36.828	-60.509	-29.729	29.584
-22.058	13.015	38.971	-51.919	37.915	-62.741	-32.140	27.632
-19.099	12.490	37.823	-48.344	38.886	-64.739	-34.102	25.670
-16.089	11.609	36.606	-44.620	39.741	-66.503	-35.701	23.816
-13.076	10.349	35.318	-40.749	40.480	-68.032	-36.987	22.128
-10.097	8.716	33.952	-36.731	41.105	-69.326	-38.004	20.649
-7.173	6.741	32.506	-32.569	41.697	-70.593	-38.784	19.327

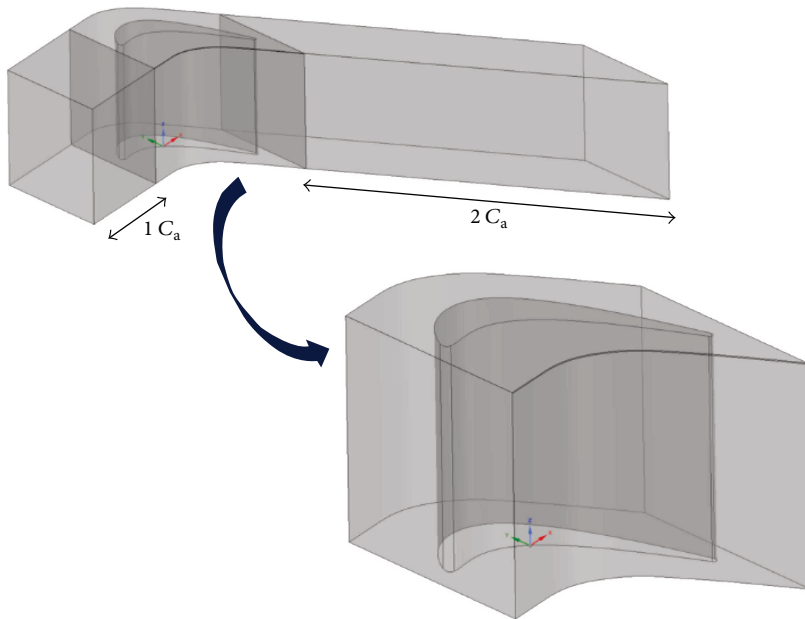


FIGURE 3: The computational domain of the linear cascade.

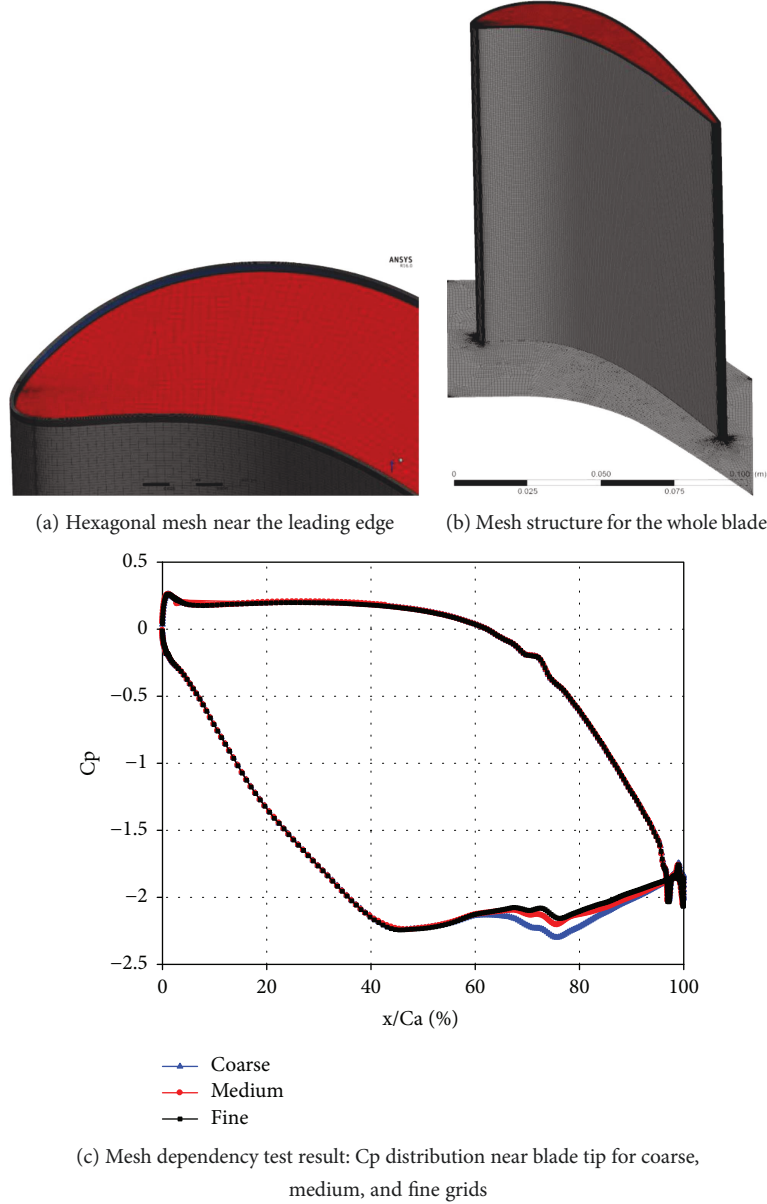


FIGURE 4: Hexagonal mesh using multizone method and mesh dependency results.

numerical calculations. In this study, y^+ has been kept at desired level around 1. In the current research, cavity and suction side squealers have been investigated numerically for a tight clearance.

Mass flow with flow angles and total temperature at the inlet and static pressure and total temperature at the outlet boundary conditions are imposed from the AFTRF test rig measurements [20]. At inlet, turbulence intensity and length scale are defined as 0.5% and 0.123 m, respectively. The maximum possible turbulent length scale was taken as the height of the blade. Uniform values in the spanwise direction are specified. For thermal boundary conditions, inlet and wall temperatures are introduced as 50°C and 25°C. 3D RANS equations for incompressible flow are solved using finite volume discretization with the assumption of steady-state flow.

A detailed validation of the specific computational method used in this paper is provided in Senel et al. [23]. Although [23] focuses on the aero-thermal influence of squealer width and height, it uses the identical tip geometry of the Axial Flow Turbine Research Facility (AFTRF) and the same computational approach used in this publication.

3. Results and Discussion

This section gives a detailed information about aerodynamic performance and the heat transfer to the blade tip surface for both cavity and suction side squealers. The numerical results for the flat tip design are also included in order to obtain a meaningful comparative understanding of relevant flow physics features.

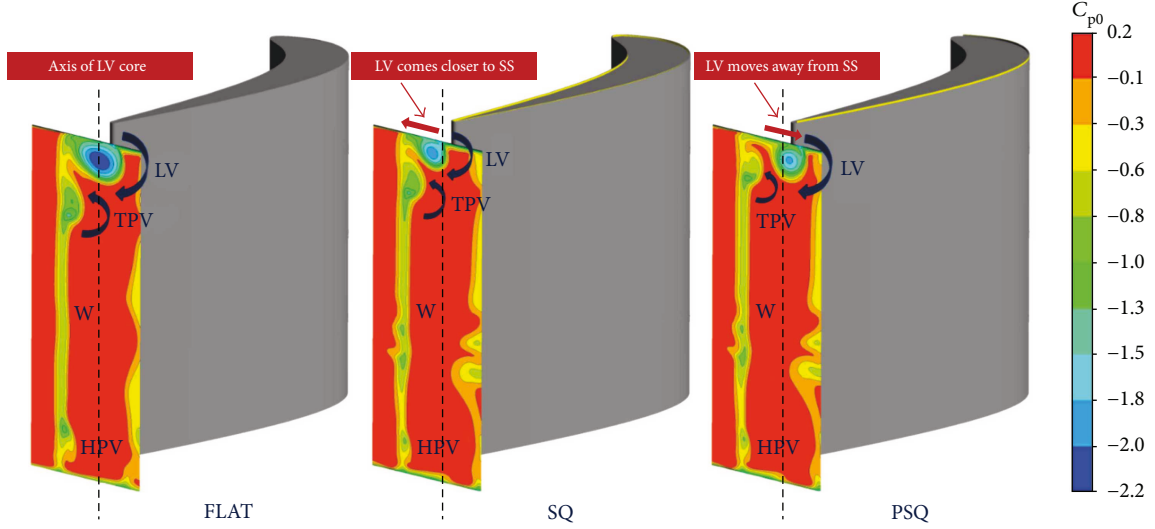


FIGURE 5: Total pressure loss coefficient at the exit plane.

4. Aerodynamic Investigation

Local total pressure loss is one of the most significant quantities to predict the performance of the blade and clarify the loss mechanisms. The numerical results for the flow structure of flat tip are taken as the baseline model. The aerodynamic performance of the squealer tip applications is compared by calculating the total pressure loss coefficient, ΔC_{p0} , at the exit plane located at $0.05C$ downstream of the rotor blade trailing edge. The total pressure loss coefficient is defined as

$$\Delta C_{p0} = \frac{\iint \rho u C_{p0} dy dz}{\iint \rho u dy dz}, \quad (1)$$

where C_{p0} is total pressure coefficient. Total pressure coefficient is defined as

$$C_{p0} = \frac{p_0 - p_{0i}}{0.5 \rho U_m^2}, \quad (2)$$

where p_{0i} is the mass-averaged total pressure at the cascade inlet and U_m is the mean blade speed at the midspan taken from AFTRF test rig operation [20]. Tip clearance of the blade, t/h , is equal to 0.5% for all cases.

ΔC_{p0} at the exit plane is plotted in Figure 5. It shows distinct regions of momentum deficits, for example, the tip leakage vortex (LV), tip passage vortex (TPV), wakes (W), and hub passage vortex (HPV). It is clearly seen that the cavity squealer (SQ) noticeably weakens the size of LV compared to the FLAT and PSQ tips. Besides, a substantial weakening is observed in the core of LV similar to Li et al. [13] and TPV for the PSQ tip. LV comes closer to the suction side of the blade due to double blockage of the cavity squealer tip as shown in Figure 5. On the other hand, LV moves away from the suction side of the blade to the pressure side of the adjacent blade for the partial squealer tip due to high momentum of leakage flow over the suction side partial squealer rim similar to experiments of Ma and Wang [18].

TABLE 3: The total pressure loss coefficient comparison.

	ΔC_{p0}	Change (%)
FLAT	0.130	—
SQ	0.126	3.08
PSQ	0.127	2.31

Table 3 provides further detail to compare the total aerodynamic performance of tip designs. Both squealer configurations provide better leakage flow control compared to the flat tip. The cavity squealer has the lowest total aerodynamic loss with 3.08% drop in ΔC_{p0} .

Figure 6 visualizes the formation of tip leakage vortex and the passage vortex as streamwise vortical systems in 3D for flat tip squealer and partial squealer tip designs, respectively. The visualization is based on postprocessing for Q criterion. The Q criterion is defined as the second invariant of the velocity gradient tensor and the positive values indicate the vortex regions [24]. The major distinction between the blade tip designs is in the location of the passage vortex. The passage vortex has been shifted upward towards the tip in spanwise direction for the partial squealer tip. Also, the use of partial squealer rims moves the tip leakage vortex away from the blade suction surface. In addition to the position of the vortical cores, there are visible differences between the magnitudes of the vortical structures. Squealer tip designs weaken the tip leakage vortex considerably. Dark blue region in the tip leakage vortex core (Figure 5) is eliminated for both squealer tip designs.

Flow visualization using streamlines in selected planes can be functional to clarify the flow structure near tip gap region. Figure 7 shows the two planes that are approximately located at $x = 0.59C$ and $x = 0.77C$. These two planes are perpendicular to the camber line. Flow passing over the pressure side rim in the tip gap results in a distinct recirculatory region. The entering pressure side flow separates near the pressure side of the cavity platform and reattaches towards

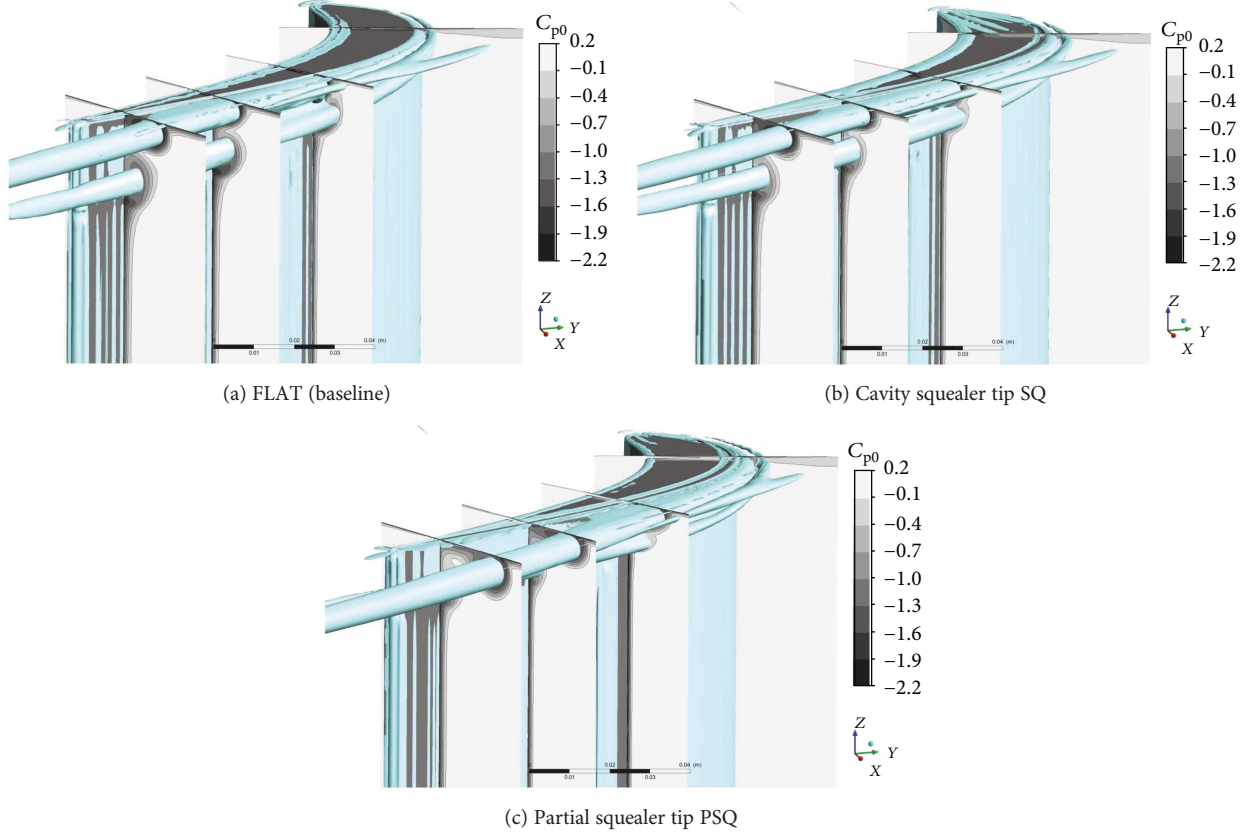
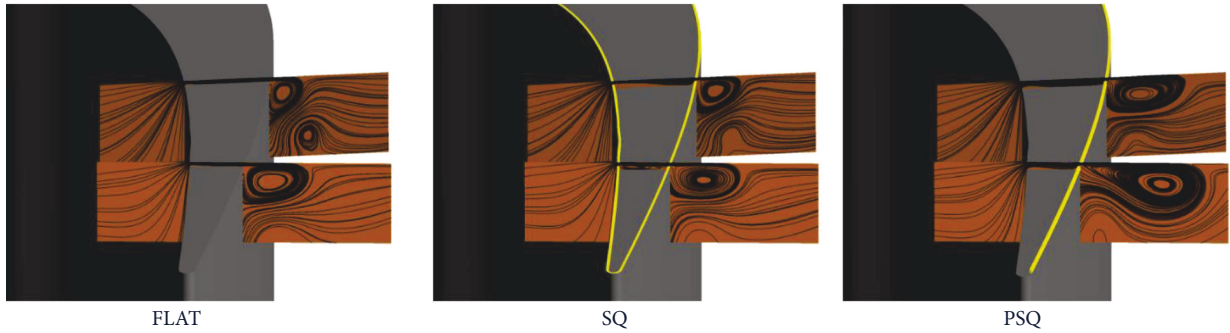


FIGURE 6: Numerically visualized vortical cores in the tip leakage zone.

FIGURE 7: Flow visualization on axially located planes, $x = 0.59C$ and $x = 0.77C$.

the camber line. Cavity squealer tips enlarge the size of this recirculatory region over the PS squealer rim. This enlarged recirculatory flow effectively blocks the net leakage flow passing over the blade tip. Then, the cavity squealer SQ imposes one more blockage against the flow passing over the SS squealer rim. The cavity squealer effectively provides a sealing mechanism to the leakage flow by means of double blockage. A wider recirculation zone formation for the SQ can be seen in Figure 7. It was observed that the area coverage of the region occupied by the tip leakage vortex decreased for the SQ but increased for the PSQ, near the suction side contour of the tip profile. Figure 7 also shows that the passage vortex TPV near the tip is measurably weakened for both squealer tips, especially for the partial squealer tip design.

One of the objectives for squealer tip geometry is to reduce leakage mass flow rate through the tip gap. Leakage flow rate at the tip gap exit is plotted in Figure 8. Leakage flow rate tends to increase up to $x = 0.9C_a$ because of the unique static pressure differential existing near the specific tip airfoil. The leakage is somewhat reduced in the last 10% of the axial chord because the static pressure on the pressure side and suction side of the tip airfoil become close to each other near the trailing edge. Although, the leakage flow distributions of the three distinct tip configurations look somewhat similar to each other, the cavity squealer configuration SQ has better performance in reducing the flow rate among all three designs. Around the trailing edge, the leakage flow rate for the flat tip corresponds to the highest values. However, the

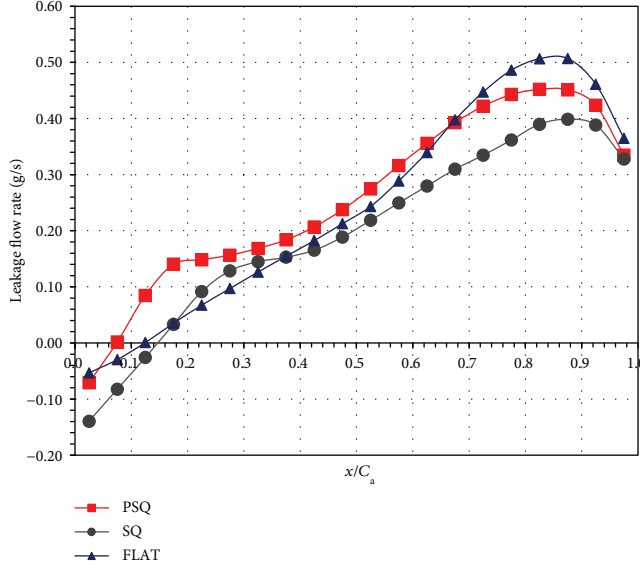


FIGURE 8: Leakage flow rate of the tip designs through the tip gap.

partial squealer tip design PSQ induces the maximum leakage in the locations from the leading edge to the $x=0.65C_a$. As shown in Table 4, cavity squealer design SQ provides a noticeable reduction of 19.0% in leakage mass flow rate. However, PSQ results in an increase in the leakage flow rate by 5.9%.

Tip clearance in the present study corresponds to tight tip clearance. Previous experimental and numerical studies show that improvement in aerodynamic performance of the current squealer tips agrees with observations in the literature, for example, Lee and Kim [14] and Schabowski and Hodson [17].

5. Thermal Investigation

The convective heat transfer coefficient on blade tip platform and squealer rim upper side is calculated for the thermal investigation. Local heat transfer coefficient is calculated as follows:

$$h = \frac{q_w''}{T_w - T_i}, \quad (3)$$

where q_w'' is wall heat flux, T_w is wall temperature, and T_i is reference temperature. T_i is calculated from mass-averaged total temperature at the inlet as suggested by Ameri and Bunker [25] and Krishnababu et al. [10]. Average heat transfer coefficient, \bar{h} , is defined as

$$\bar{h} = \frac{1}{A} \int h dA, \quad (4)$$

where A is the area of the blade tip and squealer upper wall.

The averaged heat transfer coefficient of the flat tip is calculated to be $367.8 \text{ W/m}^2 \text{ K}$ as shown in Table 5. Both squealer tip designs reduced the heat transfer to the blade tip considerably. While cavity squealer drops \bar{h} by 24.4%, partial squealer drops \bar{h} by 34.3% when compared to the flat tip.

TABLE 4: The leakage flow rate comparison.

	$\dot{m}_l (\text{g/s})$	Change (%)
FLAT	4.835	□
SQ	3.915	-19.0
PSQ	5.122	+5.9

□ relative change in reference to.

TABLE 5: The averaged heat transfer coefficient comparison.

	$\bar{h} (\text{W/m}^2 \text{ K})$	Change (%)
FLAT	367.8	□
SQ	277.9	-24.4
PSQ	241.6	-34.3

□ relative change in reference to.

Local heat transfer coefficient distribution at the blade tip reveals that PSQ performs slightly better than SQ (Figure 9). Suction side squealer provides a better cooling at blade tip surface. Locally high heat transfer regions are observed just downstream of the pressure side corner for the flat tip.

Just after the pressure side corner, the local flow goes through a vena contracta region and a small separation zone, as indicated by the yellow zone in Figure 9. After the small separation zone, the leakage flow tends to reattach on the flat tip platform generating the relatively high heat transfer coefficients around $540 \text{ W/m}^2 \text{ K}$ (brown-red). This is due to the vortical flow structures existing on the cavity platform. Leakage flow is observed to have an impingement effect at this region. Therefore, locally high heat transfer regions have been observed towards camber line of the blade. High heat transfer regions near the leading edge for cavity squealer SQ are due to formation of two different vortices. As the flow passes over the leading edge, it impinges on the blade tip surface in and separates into two flow paths. Because of this highly recirculatory impingement zone very near the leading-edge radius, thermal transport is enhanced and locally high heat transfer regions are encountered. This high heat transfer zone appears in the form of a horseshoe on all three platforms. The highest heat transfer coefficients are encountered in these red areas ($600 \text{ W/m}^2 \text{ K}$). Similar flow structures have been determined both numerically and experimentally in the literature.

Figure 10 shows the heat transfer coefficient distribution on the blade tip platform simultaneously with vertical gas side flow structures. High heat transfer regions on the blade tip due to the reattachment of the leakage flow are clarified using Q criterion. Also, vortex structure makes a better understanding for the entrance effect over the pressure side where most of the leakage fluid originates. The conventional horseshoe vortex in the gas side is also very clear near the leading-edge circle of all three designs presented in Figure 10.

6. Summary and Conclusions

A numerical study of aerodynamic loss and heat transfer for different squealer tip geometries has been presented. Detailed CFD results indicate that squealer tip designs are in general

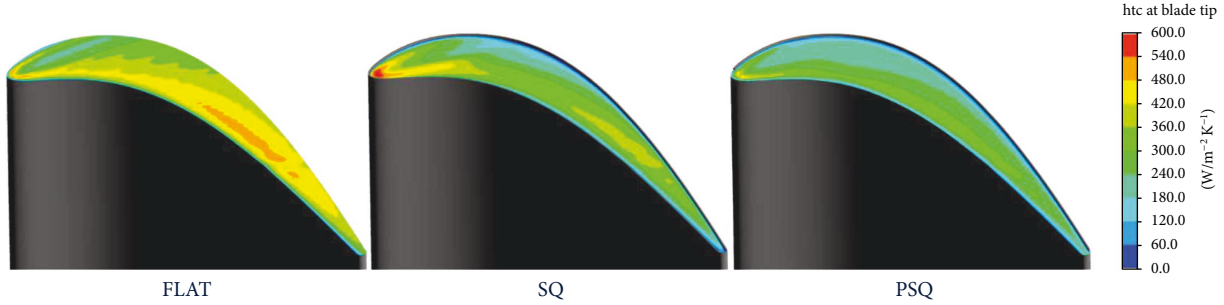


FIGURE 9: Local heat transfer coefficient distribution at blade tip.

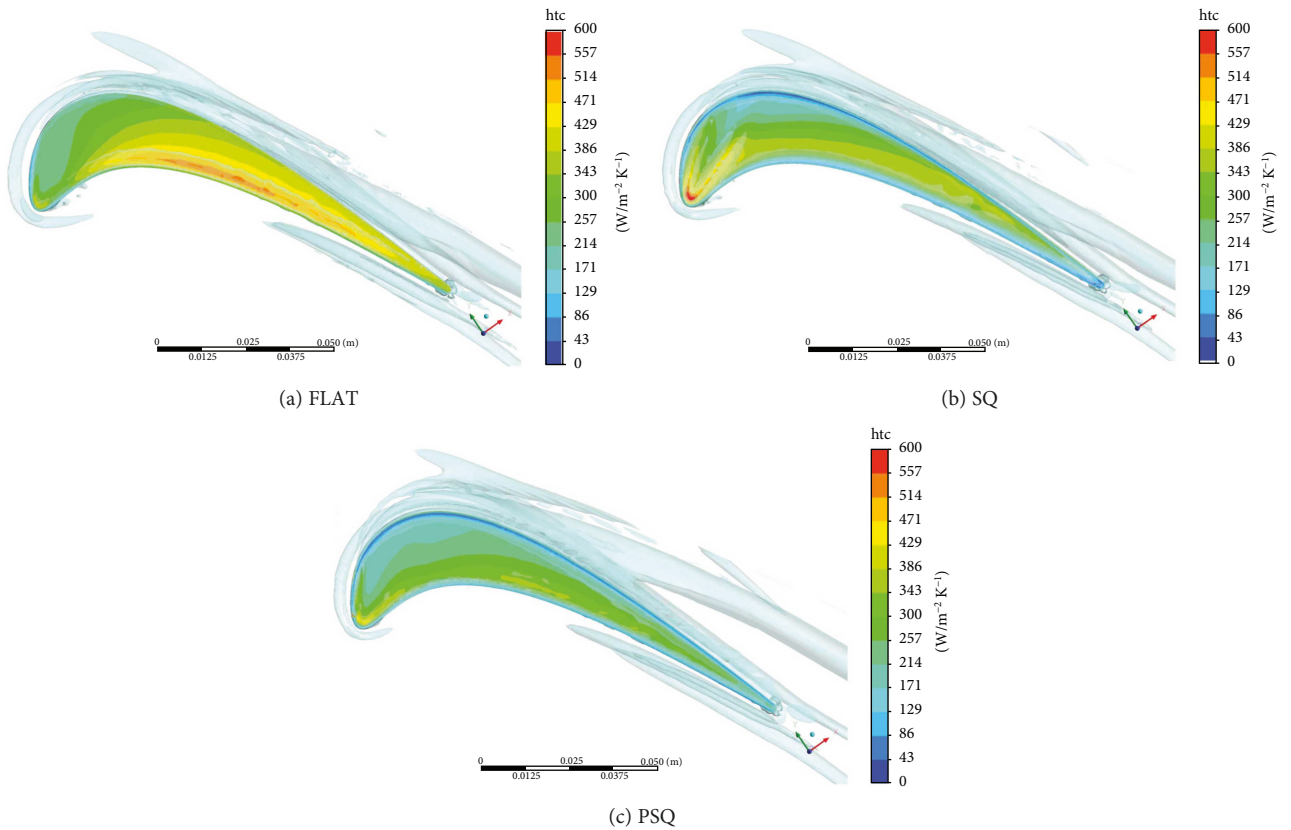


FIGURE 10: Heat transfer coefficient distribution on blade tip visualized by vortex cores.

effective to reduce aerodynamic loss and heat transfer to turbine blade tips. Total pressure loss coefficient and heat transfer coefficient are considered to interpret the numerical results. Cavity squealer SQ has better aerodynamic performance compared to the partial squealer tip design PSQ. Both squealer designs have reduced the total pressure loss with respect to the flat tip geometry. Leakage flow rate was reduced by the cavity squealer tip SQ, whereas an increase was calculated for the suction side squealer. There has not been a notable improvement in aerodynamic performance for the suction side squealer PSQ. However, a significant reduction has been achieved in heat transfer coefficients. The partial squealer tip design PSQ has provided a better thermal performance compared to the cavity squealer SQ.

Both squealer designs provided a measurable reduction in heat transfer, whereas the suction side squealer PSQ had the best heat transfer performance.

All three tip mitigation schemes used in this investigation revealed the existence of a horseshoe-like internal flow structure in the tip gap zone of the immediate leading-edge area. This near leading-edge-specific vortical flow system shows distinct flow separation and reattachment areas as evidenced from the computed tip surface heat transfer coefficients. The combination of this complex and three-dimensional flow system with the leakage fluid entering from the pressure side corner of the tip airfoil determines the local total pressure losses and thermal transport in the rest of the tip platform with or without squealer rims.

What passes through over the suction side rim in general is highly influenced from what happens inside the tip cavity volume. The leakage fluid mixing into the gas side flow from the suction side corner effectively controls the aerodynamic losses in the passage. The influence of the tip leakage jet in the form of a distinct streamwise vortex on the passage flow features such as secondary flows and blade wake system is strong. The final location and strength of the conventional passage vortex is highly influenced from the tip leakage flow system emanating from a specific tip design.

Temperature

Latin Symbols

C :	Chord
C_a :	Axial chord
C_{p0} :	Total pressure coefficient
h :	Blade span
h :	Local heat transfer coefficient
\bar{h} :	Averaged heat transfer coefficient
k :	Turbulent kinetic energy
\dot{m}_l :	Leakage mass flow rate
p :	Pressure, pitch
P_0 :	Total pressure
P_{0i} :	Mass-averaged total pressure at inlet
q_w :	Wall heat flux
r :	Radial
s :	Squealer rim width
t :	Squealer rim height
T :	Temperature
T_i :	Mass flow-averaged temperature at inlet
T_w :	Wall temperature
u :	Velocity
U_m :	AFTRF blade tip velocity at midspan
V :	Velocity component
x :	Axial distance
y^+ :	Dimensionless wall distance
ΔC_{p0} :	Total pressure loss coefficient.

Greek Symbols

α :	Flow angle
τ :	Tip gap height
θ :	Tangential
τ/h :	Tip clearance
ω :	Specific dissipation, angular speed
ζ :	Stagger angle.

Abbreviations

AFTRF:	Axial Flow Turbine Research Facility
HPV:	Hub passage vortex
LE:	Leading edge
PS:	Pressure side
RANS:	Reynolds-averaged Navier-Stokes
LV:	Tip leakage vortex
TPV:	Tip passage vortex
SS:	Suction side.

Conflicts of Interest

The authors declare that there is no conflict of interest regarding the publication of this paper.

Acknowledgments

This research was funded by the TAI-Turkish Aerospace Industries Inc. (Grant no. DKT/2014/05). The authors wish to thank TAI for the permission to publish this work. The last author Cengiz Camci also thanks the Pennsylvania State University and the Scientific and Technological Research Council of Turkey for their support during his sabbatical leave at Istanbul Technical University.

References

- [1] B. Mischo, T. Behr, and R. S. Abhari, "Flow physics and profiling of recessed blade tips: impact on performance and heat load," *Journal of Turbomachinery*, vol. 130, no. 2, article 021008, 2008.
- [2] F. J. G. Heyes, H. P. Hodson, and G. M. Dailey, "The effect of blade tip geometry on the tip leakage flow in axial turbine cascades," *Journal of Turbomachinery*, vol. 114, no. 3, pp. 643–651, 1992.
- [3] N. L. Key and T. Arts, "Comparison of turbine tip leakage flow for flat tip and squealer tip geometries at high-speed conditions," *Journal of Turbomachinery*, vol. 128, no. 2, pp. 213–220, 2004.
- [4] J. Moore and J. S. Tilton, "Tip leakage flow in a linear turbine cascade," *Journal of Turbomachinery*, vol. 110, no. 1, pp. 18–26, 1988.
- [5] J. P. Bindon, "The measurement and formation of tip clearance loss," *Journal of Turbomachinery*, vol. 111, no. 3, pp. 257–263, 1989.
- [6] M. I. Yaras and S. A. Sjolander, "Prediction of tip-leakage losses in axial turbines," *Journal of Turbomachinery*, vol. 114, no. 1, pp. 204–210, 1992.
- [7] A. A. Ameri, E. Steinþorsson, and D. L. Rigby, "Effect of squealer tip on rotor heat transfer and efficiency," *Journal of Turbomachinery*, vol. 120, no. 4, pp. 753–759, 1998.
- [8] P. J. Newton, G. D. Lock, S. K. Krishnababu et al., "Heat transfer and aerodynamics of turbine blade tips in a linear cascade," *Journal of Turbomachinery*, vol. 128, no. 2, pp. 300–309, 2004.
- [9] C. Camci, D. Dey, and L. Kavurmacioglu, "Aerodynamics of tip leakage flows near partial squealer rims in an axial flow turbine stage," *Journal of Turbomachinery*, vol. 127, no. 1, pp. 14–24, 2005.
- [10] S. K. Krishnababu, P. J. Newton, W. N. Dawes et al., "Aero-thermal investigations of tip leakage flow in axial flow turbines—Part I: effect of tip geometry and tip clearance gap," *Journal of Turbomachinery*, vol. 131, no. 1, article 011006, 2008.
- [11] L. Kavurmacioglu, D. Dey, and C. Camci, "Aerodynamic character of partial squealer tip arrangements in an axial flow turbine. Part I: detailed aerodynamic field modifications via three dimensional viscous flow simulations around baseline tip," *Progress in Computational Fluid Dynamics, An International Journal*, vol. 7, no. 7, pp. 363–373, 2007.
- [12] L. Kavurmacioglu, D. Dey, and C. Camci, "Aerodynamic character of partial squealer tip arrangements in an axial flow

- turbine. Part II: detailed numerical aerodynamic field visualisations via three dimensional viscous flow simulations around a partial squealer tip,” *Progress in Computational Fluid Dynamics, An International Journal*, vol. 7, no. 7, pp. 374–386, 2007.
- [13] W. Li, W.-y. Qiao, K.-f. Xu, and H.-l. Luo, “Numerical simulation of tip clearance flow passive control in axial turbine,” *Journal of Thermal Science*, vol. 17, no. 2, pp. 147–155, 2008.
 - [14] S. W. Lee and S. U. Kim, “Tip gap height effects on the aerodynamic performance of a cavity squealer tip in a turbine cascade in comparison with plane tip results: part 1—tip gap flow structure,” *Experiments in Fluids*, vol. 49, no. 5, pp. 1039–1051, 2010.
 - [15] C. Zhou and H. Hodson, “Squealer geometry effects on aero-thermal performance of tip-leakage flow of cavity tips,” *Journal of Propulsion and Power*, vol. 28, no. 3, pp. 556–567, 2012.
 - [16] J.-J. Liu, P. Li, C. Zhang, and B.-T. An, “Flowfield and heat transfer past an unshrouded gas turbine blade tip with different shapes,” *Journal of Thermal Science*, vol. 22, no. 2, pp. 128–134, 2013.
 - [17] Z. Schabowski and H. Hodson, “The reduction of over tip leakage loss in unshrouded axial turbines using winglets and squeezers,” *Journal of Turbomachinery*, vol. 136, no. 4, article 041001, 2013.
 - [18] H. Ma and L. Wang, “Experimental study of effects of tip geometry on the flow field in a turbine cascade passage,” *Journal of Thermal Science*, vol. 24, no. 1, pp. 1–9, 2015.
 - [19] H. Maral, C. B. Senel, L. Kavurmacioglu, and C. Camci, “Aero-thermal performance of partial and cavity squealer tip in a linear turbine cascade,” in *Proceedings of the 2nd International Conference on Advances in Mechanical Engineering*, Istanbul, Turkey, May 2016.
 - [20] C. Camci, *A Turbine Research Facility to Study Tip Desensitization Including Cooling Flows*, von Karman Institute Lecture Series, VKI-LS 2004-02, , pp. 1–26, Brussels, 2004.
 - [21] ANSYS Meshing, *16.0 Introduction to Meshing Methods: Lecture 4*, ANSYS, Inc., Canonsburg, PA, USA, 2016.
 - [22] ANSYS CFX, *16.0 Introduction to Turbulence: Lecture 10*, ANSYS, Inc., Canonsburg, PA, USA, 2016.
 - [23] C. B. Senel, H. Maral, L. A. Kavurmacioglu, and C. Camci, “An aero-thermal study of the influence of squealer width and height near a HP turbine blade,” *International Journal of Heat and Mass Transfer*, vol. 120, pp. 18–32, 2018.
 - [24] J. C. Hunt, A. A. Wray, and P. Moin, *Eddies, Streams, and Convergence Zones in Turbulent Flows*, 1988, <http://adsabs.harvard.edu/abs/1988stun.proc..193H>.
 - [25] A. A. Ameri and R. S. Bunker, “Heat transfer and flow on the first-stage blade tip of a power generation gas turbine: part 2—simulation results,” *Journal of Turbomachinery*, vol. 122, no. 2, pp. 272–277, 1999.

